RETRIEVAL OF SUGARCANE LEAF AREA INDEX FROM PRISMA HYPERSPECTRAL DATA

S. Hamzeh [1], M. Hajeb [1, *], S. K. Alavipanah [1], J. Verrelst [2]

[1] Department of Remote Sensing and GIS, Faculty of Geography, University of Tehran, Tehran, Iran - (saeid.hamzeh, m.hajeb, salavipa) @ut.ac.ir
[2] Image Processing Laboratory (IPL), Parc Científic, Universitat de Val`encia, Val`encia, Spain - (jochem.verrelst@uv.es)

Commission VI, WG VI/3

KEY WORDS: PRISMA, Leaf Area Index, Bayesian Regularized Artificial Neural Network, Hyperspectral, Sugarcane, Bootstrapping.

ABSTRACT:

The PRecursore IperSpettrale della Missione Applicativa (PRISMA) satellite of the Italian Space Agency, lunched in 2019, has provided a new generation source of hyperspectral data showing to have high potential in vegetation variable retrieval. In this study, the newly available PRISMA spectra were exploited to retrieve Leaf Area Index (LAI) of sugarcane using a new kind of Artificial Neural Networks (ANN) so-called Bayesian Regularized Artificial Neural Network (BRANN). The suggested BRANN retrieval model was implemented over a dataset collected during a field campaign in Amir Kabir Sugarcane Agro-Industrial zone, Khuzestan, Iran, in 2020. Principle Component Analysis (PCA) was utilized to reduce the dimensionality of PRISMA data cube. An accuracy assessment based on the bootstrapping procedure indicated RMSE of 0.67 m^2/m^2 for the LAI retrieval by applying the BRANN model. This study is a confirmation of the high performance of the BRANN method and high potential of PRISMA images to retrieve sugarcane LAI.

1. INTRODUCTION

Leaf Area Index (LAI) is a biophysical vegetation variable that is of great importance in the mass and energy exchanges between the Earth and the atmosphere (Bacour et al., 2006). LAI is also a very good indicator of growth and yield of crops. Sugarcane as an economic crop, cultivated in tropical and subtropical regions, provides more than half of the global demand for sugar (Som-Ard et al., 2021). Therefore, cultivating this crop with more productivity can help to improve global food security. An efficient way to increase crop productivity is to evaluate plant health status which can be done by monitoring its biophysical/chemical variables. LAI is one of the most important variables among them, so that many sugarcane growth models use it as an adjusting factor to model sugarcane growth and predict its yield (Teruel et al., 1997).

Due to its wide spatial coverage and revisit ability, remote sensing has proven to have high potential in retrieving vegetation characteristics at local and global scales (Sellers et al., 1997; Verstraete et al., 1996; Weiss et al., 2020). Statistical-empirical (regression-based) approaches are known as an easy but efficient way which are used to retrieve vegetation traits from remote sensing data. A review on application of various regression methods in the field of vegetation variable retrieval was included in (Verrelst et al., 2019).

One of the most popular non-linear non-parametric regression models is Artificial Neural Networks (ANNs) (Verrelst et al., 2015), which is frequently applied to discover relationships between remotely sensed data as independent variables and vegetation properties as target variables (see review in (Kimes et al., 1998)). Studies in which ANNs were applied to retrieve LAI have been reviewed in (Fang et al., 2019). ANNs, however, are prone to be over-fitted (Kimes et al., 2000), when the number of independent variables is large (such as what we encounter in hyperspectral images) and the number of samples is small, i.e. less than 100 , according to (Atzberger et al., 2003). Overfitting greatly reduces the generalizability of ANNs (Wang et al., 2009). To deal with overfitting problem and increase the ANNSs generalizability, regularization methods have been developed. Bayesian regularization (MacKay, 1992) is one of the most well-known regularization methods, which provides high efficiency in improving the generalizability of ANNs (Okut, 2016). Applying the Bayesian approach to regulate ANNs, Bayesian regularized ANN (BRANN) technique was developed. BRANN was applied in various fields such as environmental studies (Ye et al., 2021; Lwin et al., 2020), economy (Sariev and Germano, 2020; Yan et al., 2017) and social studies (Kayri, 2016). In the field of vegetation studies, BRANN was used to identify diseases in rice leaves (Kumar Sethy et al., 2019), and model water status of grapevine (Pôças et al., 2017). Despite the high efficiency of the BRANN method in various fields, there is still no report on its application in the field of vegetation variable retrieval from remote sensing data (Verrelst et al., 2019).

Launched in 2019, the PRISMA satellite (Loizzo et al., 2019) provides one of the most recent sources of hyperspectral data. The capability of PRISMA images in retrieving different vegetation parameters has been investigated in several studies. Tagliabue et al. (2022) used a hybrid approach based on the PROSAIL-PRO radiative transfer model and the Gaussian process regression algorithm to retrieve several vegetation variables including nitrogen, chlorophyll and water content at both leaf and canopy level from PRISMA images. They claimed the high accuracy and consistency of their results indicated the high capability of space-borne hyperspectral images in crop monitoring. Verrelst et al. (2021) used PRISMA data to map canopy nitrogen content. In that paper, the superiority of using

* Corresponding author

https://doi.org/10.5194/isprs-annals-X-4-W1-2022-271-2023

hyperspectral data against multispectral data for retrieving nitrogen content was mentioned. Casa et al. (2020) compared the capability of PRISMA hyperspectral images and Sentinel-2 multispectral images to retrieve LAI and leaf chlorophyll content using machine learning methods. Their results indicated a higher efficiency of hyperspectral images than multispectral ones, especially in case of retrieving leaf chlorophyll content.

The main aim of this paper is to regulate the ANN model using Bayesian regularization method and apply the regularized model over PRISMA hyperspectral spectra in order to retrieve LAI of sugarcane plant.

2. MATERIALS AND METHODS

2.1 Used Data

2.1.1 Field Data: The ground measurements of LAI, were carried out in seven dates from 30th May to 23th August 2020. LAI measurement was performed through a destructive manner. For this purpose, first, elementary sampling units (ESU) with size of 3 m ×1.83 m were selected. In each ESU, three plant samples that were a suitable representative for the ESU were harvested and then scanned to determine their one-sided leaf surface. The total area of the sugarcane leaves in the ESU was then calculated by multiplying the samples leaf area by the number of plants in the ESU which was counted during the fieldwork, and dividing the result by 3 (the number of samples). LAI (m^2/m^2) was finally calculated by dividing the total area of leaves by the ESU area (i.e. 5.49 m^2). The LAI measurement was performed in the number of 118 ESUs. The position of the ground measurement samples is shown in Figure 1.

2.1.2 Earth Observation Data

The PRISMA (PRecursore IperSpettrale della Missione Applicativa) satellite was launched by the Italian Space Agency on March 22, 2019 (Loizzo et al., 2019). This satellite includes a hyperspectral sensor that can capture images in 239 continuous spectral bands with a spectral resolution of less than 12 nm in the range of 400 to 2500 nm. Of these spectral bands, 66 bands are in the visible-near-infrared (VNIR) range and 173 bands are in the short-wave infrared (SWIR) range. Of course, the VNIR and SWIR ranges have a spectral overlapping between 930 nm to 1034 nm. In terms of spatial resolution, PRISMA satellite is able to acquire images with a pixel size of 30 m. This satellite also has a panchromatic (PAN) camera with a resolution of 5 m. The re-visit time of PRISMA in nadir view is 29 days, which can be shortened by up to 7 days by managing the off-nadir viewing angle (Vangi et al., 2021). PRISMA hyperspectral sensor is a pushbroom imaging spectrometer (ASI, 2020).

The PRISMA images are available in three levels of pre-processing. The level 0 (L0) product contains the raw data in binary files including auxiliary satellite data such as the cloud coverage percentage. The level 1 product (L1) contains the Top-of-Atmosphere radiance images. Level 2 products (L2) are divided into three categories. L2B is corresponding to bottom-of atmosphere radiance; L2C is ground reflectance without geometric correction, and L2D is corresponding to geocoded ground reflectance. Level 2 products can be georeferenced with the availability of ground control points (Guarini et al., 2017). PRISMA images can be downloaded for free from http://prisma-i.it/index.php/en/ after registration. The main specifications of PRISMA satellite are given in Table 1 (ASI, 2020).

Orbit Altitude	615 km	
Swath / FOV	30 km / 2.77°	
Ground Sampling Distance	Hyperspectral	30 m
	PAN	5 m
Spectral Range	VNIR	400 – 1010 nm (66 bands)
	SWIR	920 – 2500 nm (173 bands)
	PAN	400 – 700 nm
Spectral Sampling Interval	≤ 12 nm	
Spectral Width	≤ 12 nm	
Signal-to-noise ratio (SNR)	VNIR	>200:1
	SWIR	>100:1
	PAN	> 240:1

Table1. The main specifications of PRISMA satellite.

In this study, PRISMA L2D images, acquired simultaneously or with a short time difference from the field measurements, were used to retrieve sugarcane LAI.

2.2 Bayesian Regularized Artificial Neural Network

BRANN combines three concepts: back propagation ANN, the regularization technique, and the Bayesian procedure (Yan et al., 2017). Through the regularization procedure in ANN, parameter estimates are allowed to bias to the values which are more probable. This can reduce the variance of the estimates at the expense of increment of bias, resulting in producing a smoother, and hence more general, network response (Okut, 2016). For this purpose, regularization procedure considers the model parameters (network weights and biases) to minimize the objective function. While conventional training aims to reduce only the sum squared error (E_D) as performance function in the form of $F = E_D$, a regularized method also considers a weight attenuation term (E_W) which penalizes large weights. The regularized objective function becomes a linear combination of E_D and E_W, which is written as:

$$F = \beta E_D + \alpha E_W \,, \tag{1}$$

where E_D = sum squared error
E_W = sum of squares of network weights
α, β = regularization hyper-parameters

The ratio α/β dictates the emphasis for training, and controls the effective complexity of the network solution. The larger this ratio is, the more emphasis the training places on weight decay even at the cost of network errors, resulting in a more generalized network. Inversely, if the ratio becomes smaller, then the training algorithm drives the errors smaller (Dan Foresee and Hagan, 1997). Finding the optimum values for the regularization hyper-parameters is therefore the main problem with implementing regularization. To solve this problem Bayesian regularization is one of the most efficient methods (MacKay, 1992). In BRANNs, Bayes' theorem is utilized to automatically determine the optimum regularization hyper-parameters. The task is done in a probability-based iterative manner proposed by (MacKay, 1992). This manner involves imposing specified prior probability distribution on the model parameters. Using this prior probability distribution and according to the Bayes' rule, posterior probability is defined as:

$$Posterior\ probability = \frac{Likelihood \times Prior\ probability}{Evidance} . \tag{2}$$

https://doi.org/10.5194/isprs-annals-X-4-W1-2022-271-2023

The goal is to choose the weights that maximize the posterior probability. The density function for the weights is updated according to the Bayes' rule in each iteration. The steps to determine the optimum regularization hyper-parameters by the BRANN method are summarized as follows:

i. Set an initial value of α, β and the weights (w). The values are used, after the first training step, to recover the objective function parameters.

ii. Apply the Levenberg-Marquardt algorithm to minimize the objective function Equation (1), and find the current value of w.

iii. Compute the effective number of parameters, γ, using the Gauss-Newton approximation to the Hessian matrix (H) in the Levenberg-Marquardt training algorithm as follow:

$$\gamma = m - \alpha \, Trace \, H^{-1} \tag{3}$$

where m = the total number of network weights

iv. Compute new estimates for the hyper-parameters α and β using Equations (4) and (5), respectively:

$$\alpha = \frac{\gamma}{2E_w(w)} \tag{4}$$

$$\beta = \frac{N-\gamma}{2E_D(w)} \tag{5}$$

where N = the number of training samples

v. Iterate steps ii through iv until convergence.

For more detail about BRANNs refer to (Bishop, 1995; Mackay, 1995; Neal, 2012).

2.3 Designing BRANN Architecture for LAI Retrieval

First, the standard L2D PRISMA images were pre-processed as follow. Although the L2D PRISMA images used in this study are geocoded based on the WGS-84 datum and UTM projection, zone 39N, there is still a slight shift in all images when compared to the map of the sugarcane fields provided by the Amir Kabir Agro-Industrial Company. Mzid et al. (2022) also reported a displacement of up to 5 pixels in the PRISMA images used in their study. Therefore, first, the PRISMA images was geometrically corrected using the existing maps. Since L2D PRISMA images are presented as at-surface reflectance, no additional pre-processing for atmospheric correction was performed. In the following, some bands, including bands with overlap between VNIR and SWIR and those with low signal-to-noise ratio (SNR), were removed. The reflectance values in the removed bands were interpolated using spline interpolation. The resultant spectra were then smoothed using spline smoothing function in order to reduce the system noise observed in PRISMA spectra. Finally, the bands lied in the atmospheric water absorption regions and the last portion of the SWIR were excluded from the smoothed spectra. The resultant spectra were considered as input independent variables in the retrieving process.

In order to dimension reduction of the PRISMA data cube, principal component analysis (PCA) was used and the first 20 components were considered. Some previous studies showed that the first 20 principal components (PC) are sufficient to achieve high accuracy in estimating LAI from hyperspectral data (Danner et al., 2021; De Grave et al., 2020; Rivera-Caicedo et al., 2017; Verrelst et al., 2021). As a further investigation, the LAI retrieval was performed by utilizing the 20 first principal components as input independent variables.

Since the input independent variables and output target variable are of different physical nature and hence different dynamic range, the data were standardized by linearly rescaling them into a same range, i.e. $[0\,,1]$), in order to prevent scaling factor problem. Data standardization was performed for the output variable (i.e. LAI values). In the case of independent variables, the standardization was done only for the principal components. Since the L2D PRISMA were presented as reflectance, and they are intrinsically in the range $[0\,,1]$, so no further normalization was required. Since the model generates the predicted values within the range $[0\,,1]$, an inverse process was performed to invert the standardized predicted values of LAI into its actual dynamic range.

The optimum network architecture including the number of hidden layers and the number of their neurons was determined by trial and error. Tangent sigmoid and linear transfer functions were used in hidden layer(s) and output layer, respectively. (Demuth and Beale, 2004) demonstrated that a network with this combination of transfer functions is able to approximate any continuous function well.

2.4 Bootstrapping Procedure for Accuracy Assessment

The performance of the model was assessed based on the bootstrapping procedure. For this purpose, the dataset was randomly divided into two subsets; a training set consisting of 70% of samples and a testing set consisting of the remaining 30%. The model was calibrated using the training samples and the calibrated model was evaluated against test samples. The procedure was repeated 201 times to create the bootstrap replicate datasets. The selection of this number of repetitions was based on (Steyerberg et al., 2001) recommending a repetition of 200 bootstraps. We added one more repetition in order to get an odd number since we wanted the median value (of considered accuracy assessment measures) to be produced by one of the models, participating in bootstrapping, itself. In this way, 201 different values were obtained for the used accuracy assessment measures, and their median value was considered as the accuracy of results.

3. LAI RETRIEVAL EXPERIMENT

The suggested BRANN retrieval model was implemented over a study area introduced in subsection 3.1. The experimental results of the LAI retrieval are presented in subsection 3.2.

3.1 Study Area

The study area is Amir Kabir Sugarcane Agro-Industrial zone, Khuzestan, Iran, located between 48°12'19.52"E and 48°21'22.87"E latitudes, and 30°58'21.23"N and 31° 5'37.41"N longitudes. Total area of this region is 14,000 hectares, of which about 10,000 hectares were cultivated in 2020. Area of each sugarcane farm is 25 hectares (1000 m ×250 m). All farms are irrigated with a low pressure system and they are equipped with a subsurface drainage system. The topography of the region is almost flat and the predominant soil texture is loamy clay classified as heavy soil texture. The area is climatologically semi-arid with about 266 mm annual precipitation and 2788 mm/yr annual evaporation from open pans. Maximum precipitation and evapotranspiration occur in January and August, respectively.

https://doi.org/10.5194/isprs-annals-X-4-W1-2022-271-2023

The high air temperature, and high humidity due to proximity to the Persian Gulf have made the region suitable for sugarcane cultivation. The location of the study area is depicted in Figure 1.

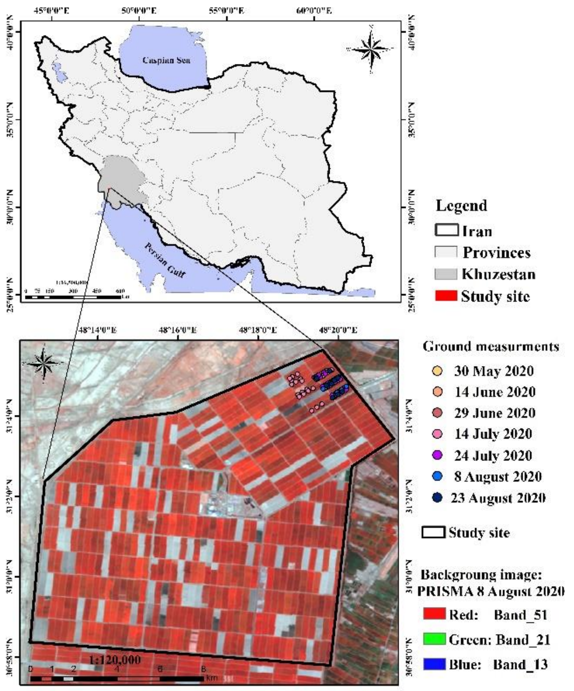

Figure 1. Study area.

3.2 Experimental Results

In the pre-processing stage, the number of 8 overlapping bands between the VNIR and SWIR ranges (i.e. 930-998 nm), as well as 80 bands with low SNR were removed. After interpolating the removed bands and smoothing the spectra using spline interpolation and smoothing, the smoothed spectra were obtained. Figure 2 shows an example of the PRISMA spectra before (blue line) and after (bold black line) gap filling and smoothing. Finally, the bands of atmospheric water absorption including 20 bands in the wavelengths of 1350 to 1510 nm and 1795 to 2000 nm, and the last portion of the SWIR between the wavelengths of 2320 to 2500 were removed and the total number of 170 smoothed bands were considered as independent variables in the retrieving process. In Figure 2, the removed bands that were excluded from retrieving process are displayed as shaded grey columns.

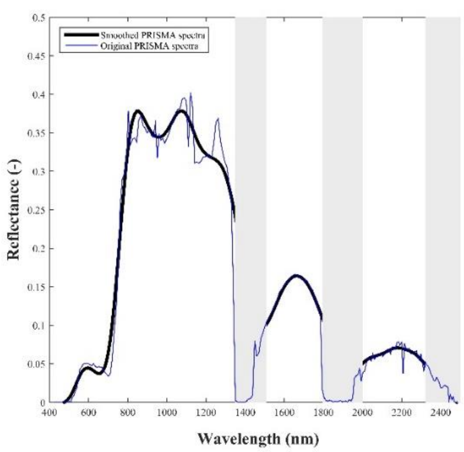

Figure 2. Example of the PRISMA spectra before and after the spline smoothing.

The results were assessed based on comparing the LAI retrievals and their corresponding ground measurements in terms of RMSE and MBE measures. The median value of the accuracy assessment measures obtained from the 201 bootstrap repetitions was considered as the accuracy of the LAI retrievals. Figure. 3 compares the performance of BRANN predictions applying the 170 smoothed PRISMA spectra with that obtained using the 20 first PCs. As seen in Fig. 3, the RMSE value of LAI retrieval was 0.67 m^2/m^2 and 0.72 m^2/m^2 applying the 170 smoothed PRISMA spectra and the 20 first PCs, respectively. Though the BRANN method could provide reasonable results in retrieving sugarcane LAI in both cases, the results of using smoothed spectra were slightly superior to the results of using principal components. This can be attributed to the fact that thanks to the penalizing large weights, BRANN can exploit more input variables without overfitting.

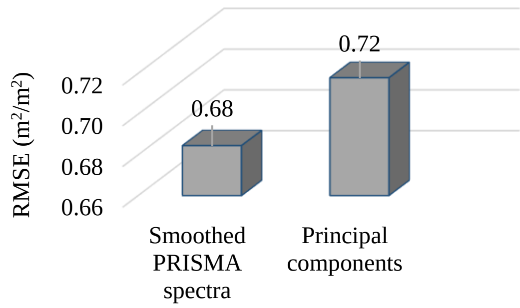

Figure 3. RMSE of sugarcane LAI retrievals.

The MBE value of LAI retrieval was 0.003 m^2/m^2 applying the 170 smoothed PRISMA spectra and -0.01 m^2/m^2 applying the 20 first PCs. The low values of MBE obtained in both cases indicate that, generally, the retrievals were on average neither underestimated nor overestimated.

Figure 4 presents the total time elapsed to BRANN retrievals of LAI by applying the smoothed PRISMA spectra and PCs. As it can be seen in this figure, the use of principal components as input variables has led to a significant reduction in computational time compared to using smoothed spectra. The computational times given here is based on using a core i5-4460 3.20 GHz personal computer with 8GB installed memory (RAM).

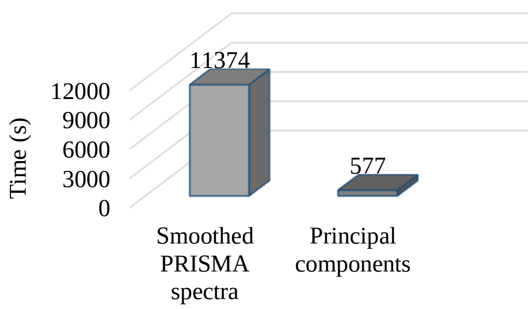

Figure 4. Computational time of sugarcane LAI retrievals.

The BRANN model with the smoothed PRISMA spectra as input variables was implemented over the acquired PRISMA images to map sugarcane LAI. For this purpose, among the 201 models participating in the bootstrapping process, the model that provided the median value of RMSEs was applied. Figure 5 displays the resulting LAI maps. As it can be seen in this figure, the LAI maps are well matched to the spatial pattern of the sugarcane fields. The LAI variations within the fields due to irrigation, fertilization or harvesting are also well reflected in the maps. Fallow fields are separated from other fields by low LAI values. Outside the Amir Kabir Sugarcane Agro-Industrial zone, there are some farms or relatively low-density vegetated areas that their spatial pattern can be clearly observed in the maps. For bare soil and non-vegetated areas close to zero and sometimes negative values have been estimated. In general, it can be said that the LAI maps represent the LAI spatial variations well in the study area.

Comparing the LAI values estimated on different dates shows the increasing trend of the LAI during the sugarcane growing season can be clearly observed. The increasing trend of LAI is also observed in the case of the farms outside the Amir Kabir Sugarcane Agro-Industrial zone. Therefore, it can be stated that the LAI maps reasonably represent the LAI temporal variations of this variable.

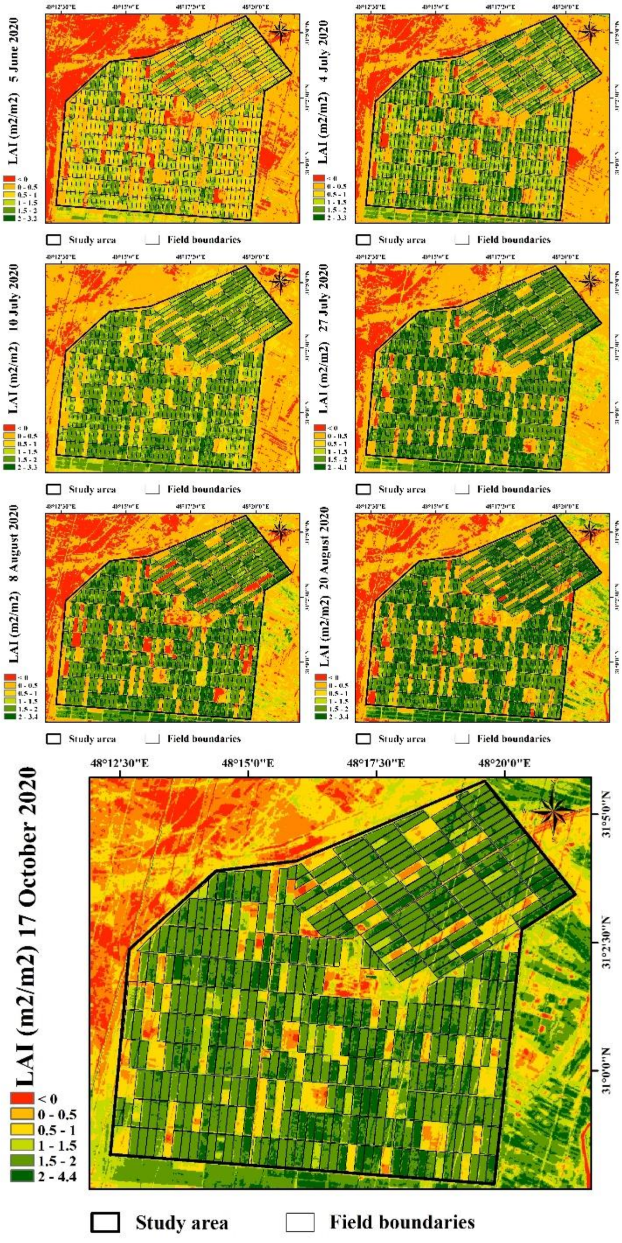

Figure 5. The maps of sugarcane LAI predicted from the PRISMA images.

4. CONCLUSION

In this paper, retrieval of LAI of sugarcane, as an important product in the food industry, from hyperspectral data cube of the PRISMA satellite was carried out by applying Artificial Neural Networks. ANN is one of the machine learning techniques that is widely used in various fields due to their high ability to discover non-linear relationships between independent and target variables. However, ANNs encounter to overfitting problem which reduces their generalizability. In this study, the Bayesian regularization method was used, in which Bayes' theorem is incorporated to overcome the overfitting problem and increase the generalizability of the model. The results indicated that the BRANN method could provide reasonable results in retrieving sugarcane LAI applying both smoothed PRISMA spectra and principal components. While using the smoothed PRISMA spectra the retrievals were slightly superior to those obtained by using the principal components, however, the use of the principal components has led to a significant reduction in computational time. This can be of significant interest within operational processing chains in which the processing time becomes important.

Visual interpretation of the generated LAI maps indicated that the LAI predictions using BRANN reasonably represent the spatial and temporal variations of sugarcane LAI.

In short, the results of this research show the high capability of the BRANN model as well as the hyperspectral images of the PRISMA satellite in retrieving sugarcane LAI.

ACKNOWLEDGEMENTS

The authors are thankful to the Amir Kabir Sugarcane Agro-Industry Company for providing the ground measurement data and maps of sugarcane fields in the study area.

REFERENCES

ASI, 2020. PRISMA Product Specifications 1–262.

Atzberger, C., Jarmer, T., Schlerf, M., Kötz, B., Werner, W., 2003. Spectroradiometric determination of wheat bio-physical variables: comparison of different empirical-statistical approaches. Remote Sens. Transitions, Proc. 23rd EARSeL Symp. Belgium 2–5.

Bacour, C., Baret, F., Béal, D., Weiss, M., Pavageau, K., 2006. Neural network estimation of LAI, fAPAR, fCover and LAI×Cab, from top of canopy MERIS reflectance data: Principles and validation. Remote Sens. Environ. 105, 313–325. https://doi.org/https://doi.org/10.1016/j.rse.2006.07.014

Bishop, C.M., 1995. Neural networks for pattern recognition. Oxford university press.

Casa, R., Upreti, D., Palombo, A., Pascucci, S., Yang, H., Yang, G., Huang, W., Pignatti, S., 2020. Evaluation and exploitation of retrieval algorithms for estimating biophysical crop variables using Sentinel-2, Venµs and PRISMA satellite data. J. Geod. Geoinf. Sci. 3, 79–88. https://doi.org/10.11947/j.JGGS.2020.0408

Dan Foresee, F., Hagan, M.T., 1997. Gauss-Newton approximation to bayesian learning, in: IEEE International

Conference on Neural Networks - Conference Proceedings. pp. 1930–1935. https://doi.org/10.1109/ICNN.1997.614194

Danner, M., Berger, K., Wocher, M., Mauser, W., Hank, T., 2021. Efficient RTM-based training of machine learning regression algorithms to quantify biophysical & biochemical traits of agricultural crops. ISPRS J. Photogramm. Remote Sens. 173, 278–296. https://doi.org/https://doi.org/10.1016/j.isprsjprs.2021.01.017

De Grave, C., Verrelst, J., Morcillo-Pallarés, P., Pipia, L., Rivera-Caicedo, J.P., Amin, E., Belda, S., Moreno, J., 2020. Quantifying vegetation biophysical variables from the Sentinel-3/FLEX tandem mission: Evaluation of the synergy of OLCI and FLORIS data sources. Remote Sens. Environ. 251, 112101. https://doi.org/10.1016/j.rse.2020.112101

Demuth, H., Beale, M., 2004. Neural Network Toolbox - For Use with MATLAB. Matlab.

Fang, H., Baret, F., Plummer, S., Schaepman-Strub, G., 2019. An Overview of Global Leaf Area Index (LAI): Methods, Products, Validation, and Applications. Rev. Geophys. 57, 739–799. https://doi.org/10.1029/2018RG000608

Guarini, R., Loizzo, R., Longo, F., Mari, S., Scopa, T., Varacalli, G., 2017. Overview of the prisma space and ground segment and its hyperspectral products, in: International Geoscience and Remote Sensing Symposium (IGARSS). pp. 431–434. https://doi.org/10.1109/IGARSS.2017.8126986

Kayri, M., 2016. Predictive abilities of Bayesian regularization and levenberg-marquardt algorithms in artificial neural networks: A comparative empirical study on social data. Math. Comput. Appl. 21, 20. https://doi.org/10.3390/mca21020020

Kimes, D.S., Knyazikhin, Y., Privette, J.L., Abuelgasim, A.A., Gao, F., 2000. Inversion methods for physically-based models. Remote Sens. Rev. 18, 381–439. https://doi.org/10.1080/02757250009532396

Kimes, D.S., Nelson, R.F., Manry, M.T., Fung, A.K., 1998. Attributes of neural networks for extracting continuous vegetation variables from optical and radar measurements. Int. J. Remote Sens. 19, 2639–2663. https://doi.org/10.1080/014311698214433

Kumar Sethy, P., Kanta Barpanda, N., Rath, A., Sethy, P.K., Patel, K., Rath, A.K., 2019. BRANN Model for Identification of Rice Leaf Diseases Using Texture Feature Wireless Sensor Network View project Agricultural Image Processing View project BRANN Model for Identification of Rice Leaf Diseases Using Texture Feature 569.

Loizzo, R., Daraio, M., Guarini, R., Longo, F., Lorusso, R., DIni, L., Lopinto, E., 2019. Prisma Mission Status and Perspective, in: International Geoscience and Remote Sensing Symposium (IGARSS). pp. 4503–4506. https://doi.org/10.1109/IGARSS.2019.8899272

Lwin, A., Yang, D., Hong, X., 2020. Leveraging Bayesian Deep Learning for Spaceborne GNSS-R Retrieval on Global Soil Moisture, in: 2020 International Conference on Artificial Intelligence in Information and Communication (ICAIIC). IEEE, pp. 352–355. https://doi.org/10.1109/ICAIIC48513.2020.9065053

Mackay, D.J.C., 1995. Probable networks and plausible predictions — a review of practical Bayesian methods for supervised neural networks. Netw. Comput. Neural Syst. 6, 469–505. https://doi.org/10.1088/0954-898X_6_3_011

MacKay, D.J.C., 1992. Bayesian Interpolation. Neural Comput. 4, 415–447. https://doi.org/10.1162/neco.1992.4.3.415

Mzid, N., Castaldi, F., Tolomio, M., Pascucci, S., Casa, R., Pignatti, S., 2022. Evaluation of Agricultural Bare Soil Properties Retrieval from Landsat 8, Sentinel-2 and PRISMA Satellite Data. Remote Sens. 14, 714. https://doi.org/10.3390/rs14030714

Neal, R.M., 2012. Bayesian learning for neural networks. Springer Science & Business Media.

Okut, H., 2016. Bayesian Regularized Neural Networks for Small n Big p Data, Artificial Neural Networks - Models and Applications. IntechOpen. https://doi.org/10.5772/63256

Pôças, I., Gonçalves, J., Costa, P.M., Gonçalves, I., Pereira, L.S., Cunha, M., 2017. Hyperspectral-based predictive modelling of grapevine water status in the Portuguese Douro wine region. Int. J. Appl. Earth Obs. Geoinf. 58, 177–190. https://doi.org/https://doi.org/10.1016/j.jag.2017.02.013

Rivera-Caicedo, J.P., Verrelst, J., Muñoz-Marí, J., Camps-Valls, G., Moreno, J., 2017. Hyperspectral dimensionality reduction for biophysical variable statistical retrieval. ISPRS J. Photogramm. Remote Sens. 132, 88–101. https://doi.org/10.1016/j.isprsjprs.2017.08.012

Sariev, E., Germano, G., 2020. Bayesian regularized artificial neural networks for the estimation of the probability of default. Quant. Financ. 20, 311–328. https://doi.org/10.1080/14697688.2019.1633014

Sellers, P.J., Dickinson, R.E., Randall, D.A., Betts, A.K., Hall, F.G., Berry, J.A., Collatz, G.J., Denning, A.S., Mooney, H.A., Nobre, C.A., Sato, N., Field, C.B., Henderson-Sellers, A., 1997. Modeling the exchanges of energy, water, and carbon between continents and the atmosphere. Science (80-.). 275, 502–509. https://doi.org/10.1126/science.275.5299.502

Som-Ard, J., Atzberger, C., Izquierdo-Verdiguier, E., Vuolo, F., Immitzer, M., 2021. Remote sensing applications in sugarcane cultivation: A review. Remote Sens. https://doi.org/10.3390/rs13204040

Steyerberg, E.W., Harrell, F.E.J., Borsboom, G.J., Eijkemans, M.J., Vergouwe, Y., Habbema, J.D., 2001. Internal validation of predictive models: efficiency of some procedures for logistic regression analysis. J. Clin. Epidemiol. 54, 774–781. https://doi.org/10.1016/s0895-4356(01)00341-9

Tagliabue, G., Boschetti, M., Bramati, G., Candiani, G., Colombo, R., Nutini, F., Pompilio, L., Rivera-Caicedo, J.P., Rossi, M., Rossini, M., Verrelst, J., Panigada, C., 2022. Hybrid retrieval of crop traits from multi-temporal PRISMA hyperspectral imagery. ISPRS J. Photogramm. Remote Sens. 187, 362–377. https://doi.org/10.1016/j.isprsjprs.2022.03.014

Teruel, D.A., Barbieri, V., Ferraro Jr., L.A., 1997. Sugarcane leaf area index modeling under different soil water conditions. Sci. Agric. 54, 39–44. https://doi.org/10.1590/s0103-90161997000300008

Vangi, E., D'amico, G., Francini, S., Giannetti, F., Lasserre, B., Marchetti, M., Chirici, G., 2021. The new hyperspectral satellite prisma: Imagery for forest types discrimination. Sensors (Switzerland). https://doi.org/10.3390/s21041182

Verrelst, J., Camps-Valls, G., Muñoz-Marí, J., Rivera, J.P., Veroustraete, F., Clevers, J.G.P.W., Moreno, J., 2015. Optical remote sensing and the retrieval of terrestrial vegetation bio-geophysical properties – A review. ISPRS J. Photogramm. Remote Sens. 108, 273–290. https://doi.org/https://doi.org/10.1016/j.isprsjprs.2015.05.005

Verrelst, J., Malenovský, Z., Van der Tol, C., Camps-Valls, G., Gastellu-Etchegorry, J.-P., Lewis, P., North, P., Moreno, J., 2019. Quantifying Vegetation Biophysical Variables from Imaging Spectroscopy Data: A Review on Retrieval Methods. Surv. Geophys. 40, 589–629. https://doi.org/10.1007/s10712-018-9478-y

Verrelst, J., Rivera-Caicedo, J.P., Reyes-Muñoz, P., Morata, M., Amin, E., Tagliabue, G., Panigada, C., Hank, T., Berger, K., 2021. Mapping landscape canopy nitrogen content from space using PRISMA data. ISPRS J. Photogramm. Remote Sens. 178, 382–395. https://doi.org/10.1016/j.isprsjprs.2021.06.017

Verstraete, M.M., Pinty, B., Myneni, R.B., 1996. Potential and limitations of information extraction on the terrestrial biosphere from satellite remote sensing. Remote Sens. Environ. 58, 201–214. https://doi.org/https://doi.org/10.1016/S0034-4257(96)00069-7

Wang, H., Ji, F., Wei, G., Leung, C., Sum, P., 2009. Regularization Parameter Selection for Faulty Neural Networks. Int. J. Intell. Syst. Technol. 1, 2–5.

Weiss, M., Jacob, F., Duveiller, G., 2020. Remote sensing for agricultural applications: A meta-review. Remote Sens. Environ. 236, 111402.

Yan, D., Zhou, Q., Wang, J., Zhang, N., 2017. Bayesian regularisation neural network based on artificial intelligence optimisation. Int. J. Prod. Res. 55, 2266–2287. https://doi.org/10.1080/00207543.2016.1237785

Ye, L., Jabbar, S.F., Abdul Zahra, M.M., Tan, M.L., 2021. Bayesian Regularized Neural Network Model Development for Predicting Daily Rainfall from Sea Level Pressure Data: Investigation on Solving Complex Hydrology Problem. Complexity 2021, 6631564. https://doi.org/10.1155/2021/6631564